Size-Dependent Properties of Sonochemically Synthesized Three-Dimensional Arrays of Close-Packed Semiconducting $AgBiS_2$ Quantum Dots

Biljana Pejova,*[,†] Ivan Grozdanov,[†] Diana Nesheva,[‡] and Anna Petrova[§]

Institute of Chemistry, Faculty of Natural Sciences and Mathematics, Saints Cyril and Methodius University, POB 162, 1000 Skopje, Macedonia, Institute of Solid State Physics, Bulgarian Academy of Sciences, 72 Tzarigradsko Chaussee Boulevard, 1784 Sofia, Bulgaria, and Space Research Institute, Bulgarian Academy of Sciences, P.O. Box 799, 1000 Sofia, Bulgaria

Received July 8, 2007. Revised Manuscript Received January 16, 2008

3D arrays of close-packed $AgBiS_2$ quantum dots (QDs) in thin film form were synthesized for the first time using novel, convenient sonochemical approach. Structural, optical, and photoelectrical properties of the synthesized material were investigated with an emphasis on their dependence on crystal size. The sonochemically synthesized $AgBiS_2$ colloidal crystals have an average QD radius of 4.2 nm, twice as small compared to the QD solid obtained without ultrasonic irradiation. The optical band gap energy of sonochemically synthesized $AgBiS_2$ QD thin films of 1.40 eV is strongly blue-shifted in comparison to that of the macrocrystal (0.90 eV) and that of nanostructured films synthesized by conventional chemical route (1.10 eV). Upon annealing, E_g exhibits a red shift to 1.00 eV. Spectral dependence of stationary nonequilibrium conductivity of the 3D QD assemblies suggests that the thin films' photoconductivity is modulated by the intercrystalline barrier height decrease. E_g of the films calculated on the basis of photoconduction spectral response in the low-absorption region is 1.18 eV. Thermal band gap energy of the films is 1.10 eV, whereas both the variable range hopping conduction and thermionic emission mechanisms are predominant in the overall intercrystalline charge carrier transport through 3D QD assemblies.

1. Introduction

In recent years, the research in the field of semiconducting materials is aimed toward development of simple, convenient and environmentally friendly methods for synthesis of nanostructured materials that exhibit unusual properties (in comparison with the corresponding bulk ones) with large potential application. The unusual behavior of low-dimensional semiconductors is closely related to their structure, which could be described simply as an intermediate state between the state of molecular entities from one viewpoint and macrocrystalline solids from another. Using the language of solid state theory, this means that as semiconductor's particle size decreases, the electronic bands of the macrocrystalline material split into discrete energy levels followed by band gap broadening.[1–8] The crystal size reducing leads to confinement of electron and hole motions inside a particle and increase of surface/volume ratio as well. In the case of small particles, the larger number (fraction) of surface atoms has an additional influence on the band structure, leading to appearance of discrete energy levels into the forbidden band. These states could also have significant effects on the semiconductor's properties. The properties of low-dimensional semiconductors change profoundly as the "characteristic length" of nanoparticles becomes comparable with the exitonic Bohr radius[1,2,8] for the corresponding bulk sample. This quantity is a natural measure of the confinement length in semiconducting materials and corresponds to the radius of electron's first orbit in the hydrogen atom described in the framework of Bohr atomic model. To emphasize the quantum character of the confinement effects, along with the nanodimensions of particle's characteristic length, researchers have coined the term "quantum dot" (QD).[1–8] The smaller the crystal size, the more manifested the size-dependent properties.

The crucial role of low-dimensional semiconducting materials in contemporary science and technology arises from the remarkable size-dependent optical and electronic structure properties that they exhibit. The mentioned size-induced band gap variation is probably the most notable among these. It enables spectral tunability of light absorption and emission as well as an enhancement of the oscillator strength induced due to quantum confinement effects. In addition to funda-

* Corresponding author. E-mail: biljana@iunona.pmf.ukim.edu.mk.
† Saints Cyril and Methodius University.
‡ Institute of Solid State Physics, Bulgarian Academy of Sciences.
§ Space Research Institute, Bulgarian Academy of Sciences.

(1) Yu, P. Y.; Cardona, M. *Fundamentals of Semiconductors*; Springer: Berlin, 1999.
(2) Seeger, K. *Semiconductor Physics*; Springer-Verlag: New York, 1997.
(3) Dalven, R. *Introduction to Applied Solid State Physics*; Plenum Press: New York, 1990.
(4) Callister, W. D. *Materials Science and Engineering*; Wiley: New York, 1997.
(5) Marder, M. P. *Condensed Matter Physics*; John Wiley & Sons: New York, 2000.
(6) West, A. R. *Basic Solid State Chemistry*; John Wiley & Sons: New York, 2000.
(7) Sze, S. M. *Semiconductor Devices: Physics and Technology*; Wiley: New York, 1985.
(8) Klingshirin, C. F. *Semiconductor Optics*; Springer: Berlin, 1997.

10.1021/cm071794k CCC: $40.75
Published on Web 03/15/2008

mental importance of nanosized materials, the exciting new physics of low-dimensional semiconductors allows their wide application in optoelectronics and nonlinear optical devices. A particularly interesting topic within this research area is related to the optical, electrical, and photophysical properties of semiconducting QDs deposited as continual thin films. In fact, an individual QD nanostructure is a zero-dimensional analogue of the two-dimensional quantum well (QW). When individual QDs are close-packed (forming, for example, three-dimensional assembly or array of QDs), further new opportunities are opened and fundamentally new aspects could be explored. In the case of 3D arrays of QDs, the collective physical phenomena, that develop upon interaction of the proximal QDs might be explored, while certain properties, which are characteristic of individual QDs are retained (see refs 9−16 and references therein). In some recent publications devoted to this subject, the terms "QD solid" or "colloidal crystal" have been used referring to 3D QD arrays, in order to emphasize that these structures correspond to a new form of organization of matter. Such unique properties characteristic of an individual QD on the one hand and the cooperative effects in QD solids on the other hand, make these novel types of superstructures very convenient media with great potential for application in optical and electronic devices. Having in mind the possibilities for their application, as well as the fundamental questions with respect to solid-state science that arise from studies of these materials, the continuously increasing interest in this area is self-understood. In this context, it is worth mentioning that even purely fundamental considerations related to physicochemical properties of low-dimensional systems may be of crucial importance for development of new technological breakthroughs. In relation to these aspects of contemporary materials science, two important issues arise concerning synthetic materials chemistry: being able to synthesize a given material with predefined (i.e., designed) properties and being able to understand the experimentally observed size-dependence of these properties.

To fulfill the first of the previously mentioned issues, various novel synthetic approaches have emerged as an alternative to conventional ones. Nowadays, in the field of semiconducting nanomaterials, there is an astonishingly growing interest for sonochemistry as a powerful synthetic tool. The origin of sonochemistry is a phenomenon of acoustic cavitation that includes formation, growth, and implosive collapse of bubbles in liquids irradiated with high-intensity ultrasound. The implosive collapse of bubbles is followed by generation of so-called hot spots with short lifetime where the conditions are extreme (for example a temperature of ∼5000 K, pressure of 1000 atm, and heating and cooling rates above 1×10^{10} K/s). The high local temperature and pressure, combined with extraordinary rapid cooling rates, provide a unique means for driving chemical reactions under extreme local conditions, in spite of the fact that the average macroscopic parameters' values characterizing the reactor are quite modest. In addition to this, when ultrasonic irradiation is applied on liquid−powder suspensions (systems in which solid–liquid phase boundaries are present), further effects can occur that lead to substantial changes in properties of the synthesized material. To distinguish these effects from those occurring in a homogeneous medium, they are usually referred to as heterogeneous sonochemical effects. At the very essence of the heterogeneous sonochemical effects is the implosive collapse of acoustically generated bubbles in the immediate vicinity of the phase boundary, leading to high-speed microjets and shockwaves. Depending on the size of particles forming the solid phase and their melting temperature, acoustically generated shockwaves and microjects may lead either to particle erosion (size decrease) or coagulation induced by local melting. Therefore, the remarkable advantages of sonochemical approach include a rapid reaction rate, controllable reaction conditions and ability to produce nanoparticles with uniform shapes, narrow size distributions, and high purities.

In this study, we present our results related to synthesis of nanostructured $AgBiS_2$ thin films and investigation of their size-dependent structural, optical, and photoelectrical properties. Having in mind the advantages of ultrasonic irradiation of the reaction system in the course of attempts to nanostructural material design, we have applied a sonochemical approach in the preparation process of $AgBiS_2$ thin films. To follow the evolution of their size-dependent properties; however, we have also synthesized thin films of the semiconductor under investigation using conventional chemical method. Our interest for this ternary semiconducting material is motivated by several reasons. First, $AgBiS_2$ belongs to the group of I−V−VI semiconducting materials, which are crucial in production of linear and nonlinear optoelectronic and thermoelectric devices, as well as in optical recording media.[17,18] Second, to the best of our knowledge, up to now the investigated semiconductor has not been synthesized in the form of a thin film, although it is technologically a very important material. In most cases, $AgBiS_2$ has been investigated from a crystallographic or thermodynamic point of view.[19,20] Extensive literature search has led us to only a few papers which deal with synthesis of the mentioned semiconductor. In a powder form, $AgBiS_2$ has been traditionally synthesized either via a solid state reaction from the corresponding elemental substances (silver,

(9) Kagan, C. R.; Murray, C. B.; Nirmal, M.; Bawendi, M. G. *Phys. Rev. Lett.* **1996**, *76*, 1517.
(10) Kagan, C. R.; Murray, C. B.; Bawendi, M. G. *Phys. Rev. B* **1996**, *54*, 8633.
(11) Gindele, F.; Westphäling, R.; Woggon, U.; Spanhel, L.; Ptatschek, V. *Appl. Phys. Lett.* **1997**, *71*, 2181.
(12) Artemyev, M. V.; Bibik, A. I.; Gurinovich, L. I.; Gaponenko, S. V.; Woggon, U. *Phys. Rev. B* **1999**, *60*, 1504.
(13) Artemyev, M. V.; Woggon, U.; Jaschinski, H.; Gurinovich, L. I.; Gaponenko, S. V. J. *Phys. Chem. B* **2000**, *104*, 11617.
(14) Artemyev, M. V.; Bibik, A. I.; Gurinovich, L. I.; Gaponenko, S. V.; Jaschinski, H.; Woggon, U. *Phys. Status Solidi B* **2001**, *224*, 393.
(15) Kim, B. S.; Islam, M. A.; Brus, L. E.; Herman, I. P. J. *Appl. Phys.* **2001**, *89*, 8127.
(16) Kim, D. E.; Islam, M. A.; Avila, L.; Herman, I. P. J. *Phys. Chem. B* **2003**, *107*, 6318.
(17) Snmanta, L. K.; Chatterjee, S. *Phys. Status Solidi B* **1994**, *182*, 85.
(18) Aliev, S. A.; Raginov, S. S. *Neorg. Mater.* **1992**, *28*, 329.
(19) Schmidt, J. A.; Sagua, A. E.; Prat, M. R. *Mater. Chem. Phys.* **1999**, *61*, 153.
(20) Gather, B.; Blachnik, R. *J. Less-Common Met.* **1980**, *70*, 11–24.

bismuth, and sulfur) or from binary chalcogenides,[21,22] whereas Chen et al. have recently synthesized for the first time nanocrystalline $AgBiS_2$ with different shape crystals, like nanorods, with diameters of about 40 nm and lengths up to 10 μm.[23] Coral-shaped[24] and dendritic crystals[25] of this material have also been recently synthesized. However, we have not found any literature data referring to $AgBiS_2$ synthesized in thin film form or to three-dimensional assemblies (arrays) constituted by QDs of this material.

Actually, the results presented in this paper are a continuation of our work in the field of semiconducting nanocrystalline thin film materials.[26–29] Here, we focus our attention mainly on synthesis of low-dimensional $AgBiS_2$ ternary semiconductor in thin film form and on the size-dependent structural, optical, and photoelectrical properties.

2. Experimental Section

Thin films of bismuth(III) silver sulfide quantum dots were synthesized using chemical and sonochemical deposition methods. In both approaches, the used reaction system was composed of the following components: silver nitrate, bismuth nitrate and sodium thiosulfate. The first two substances serve as metal ions precursors, whereas the third one plays a double role: as a complexing agent and as a sulfide ion precursor. Because the Bi^{3+} cation has a strong tendency toward hydrolysis, in order to avoid precipitation of $BiONO_3$, bismuth(III) nitrate was dissolved in a solution of nitric acid ($c(HNO_3) = 2$ mol/dm^3). A classical optimization of the experimental conditions for conventional thin film deposition was performed, aiming to produce the synthesized material with pronounced low-dimensional structure, and at the same time, to achieve maximum photoresponse characteristics. However, as explained in more details in the following chapter, the optimization of experimental conditions was actually based on previous careful consideration of both thermodynamical and kinetical factors which were expected to influence the processes of nucleation and crystal growth. It was found that high-quality homogeneous films could be deposited from reaction systems with various initial and final concentrations of the main reactant species in the reactors, as well as their molar ratios. Best photoelectrical performances of the finally synthesized 3D QD assemblies in thin film form were achieved with initial concentrations of both $AgNO_3$ and $Bi(NO_3)_3$ solutions of 0.1 mol dm^{-3}, initial concentration of $Na_2S_2O_3$ solution of 1 mol dm^{-3}, keeping the volume ratio of these three species of 1:1:1.

In the case of a sonochemical approach, we were irradiating continuously the reaction system with a high-intensity ultrasonic radiation, whereas all other experimental conditions remained unchanged. The sonification of the reaction system was performed using a direct immersion ultrasonic horn generating high-intensity ultrasound radiation (100 W/cm^2) with a frequency of 20 kHz. The influence of ultrasound radiation on the mechanism of thin film deposition process, as well as on the properties of synthesized materials will be discussed in more details later in the paper.

The synthesized semiconducting quantum dots were deposited onto standard (commercially available) microscopic glasses. The adhesion of prepared thin films with substrate's surface was improved by means of a previous treatment of used microscopic glasses. First of all, the microscopic glasses were treated with chromsulphuric acid which is a well-known oxidizing reagent, widely used for cleaning in the laboratories. Afterward, the substrates were immersed in a diluted solution of tin(II) chloride ($\omega(SnCl_2) = 0.03\%$) for about twenty minutes, than they were washed with deionized water and thermally treated at ~200–220 °C. Taking into account the chemistry of Sn^{2+} ions, the hydrolysis process of these ions is followed by creation of very small crystals of Sn(OH)Cl onto the substrate surface with stochastic distribution.[26] As it has been shown in the literature, during the air-annealing process, the obtained Sn(II) species are chemically transformed to tin(IV) species (Sn(IV) oxide). They have an important role in the course of thin film deposition, acting as nucleation centers and initiating the heterogeneous nucleation processes. Actually, in the present case, the Sn(IV) oxide is very susceptible to form sulfide species. This, in turn, helps to adhere the ternary chalcogenide thin film.

3. Thin Film Characterization

The identification of the synthesized nanostructured semiconducting thin film materials was done using X-ray diffraction analysis, whereas their optical and photoelectrical properties were investigated employing optical spectroscopy, thermoelectrical and photoelectrical measurements. XRD analysis was performed on a Philips PW 1710 diffractometer using monochromatic Cu-K_α radiation. In addition to identification, the recorded XRD patterns were employed for estimation of the average crystal radius.

The surface morphology of as-deposited films prepared by sonochemical and chemical routes was also studied by atomic force microscopy (AFM) technique. A scanning nanoindenter NanoScan (http://www.nanoscan.info/eng/index.html), a device for surface properties investigations and measurements of hardness and elastic modulus of ultra hard materials and thin films, was used operating in contact dynamic (surface topography) mode. Arrays of 1000 × 1000 pixels were taken on a scanning area of 1.0 × 1.0 μm^2.

Optical spectra of synthesized thin films were recorded on a Cary 50 spectrophotometer in the UV–vis−NIR spectral range. They were processed and analyzed using Microsoft Excel and Microcal Origin software packages.[30,31]

Electrical and photoelectrical properties were investigated using the constant-field method.[32] This method is based on electrical circuit presented in Figures 1 and 2. It is composed of a direct current source (B) serially connected to the investigated thin film sample (F) and a standard resistor (R). All electrical measurements were carried out in the region of ohmic conductivity of the samples (the linear part of the

(21) Kullerud, G.; Yoder, H. S. *Econ. Geol.* **1959**, *54*, 533.
(22) Nair, P. K.; Huang, L.; Nair, M. T. S.; Hu, H.; Meyers, E. A.; Zingaro, R. A. J. *Mater. Res.* **1997**, *12*, 651.
(23) Shen, G.; Chen, D.; Tang, K.; Qian, Y. J. *Cryst. Growth* **2003**, *252*, 199.
(24) Shen, G.; Chen, D.; Tang, K.; Qian, Y. J. *Cryst. Growth* **2003**, *257*, 293.
(25) Shen, G.; Chen, D.; Tang, K.; Jiang, X.; Huang, L.; Jin, Y.; Qian, Y. *Inorg. Chem. Commun.* **2003**, *6*, 710.
(26) Pejova, B.; Tanuševski, A.; Grozdanov, I. *J. Solid State Chem.* **2004**, *177*, 4785.
(27) Pejova, B.; Tanuševski, A.; Grozdanov, I. *J. Solid State Chem.* **2006**, *178*, 1786.
(28) Pejova, B.; Grozdanov, I. *Czech. J. Phys.* **2006**, *56*, 75.
(29) Pejova, B.; Grozdanov, I. *Thin Solid Films* **2007**, *515*, 5203.
(30) *Microsoft Excel*; Microsoft Corporation: Redmond, WA, 1985–2003.
(31) *Microcal Origin*, version 5.0; Microcal Software, Inc.: Northampton, MA, 1991–1997.
(32) Ohring, M. *The Materials Science of Thin Films*; Academic Press: New York, 1992.

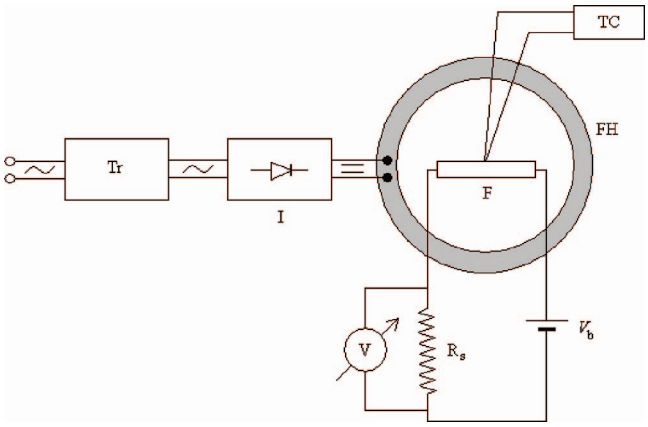

Figure 1. The experimental setup used for measurements of temperature dependence of dark electrical resistance of the synthesized 3D assemblies of $AgBiS_2$ quantum dots deposited as thin films.

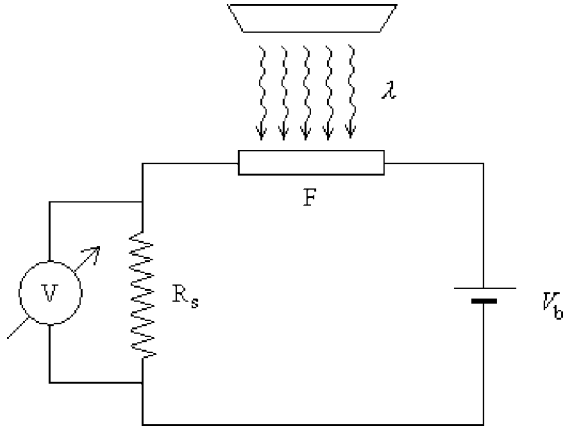

Figure 2. Experimental setup used for measurement of the spectral dependence of stationary nonequilibrium conductivity (photoconductivity) of the synthesized 3D assemblies of $AgBiS_2$ QDs deposited as thin films.

current–voltage characteristics), i.e., in the absence of effects related to large current injection directly from the electrodes (the space-charge limited current, SCLC). Taking into account Ohm's law, from the analysis of the mentioned circuit, the following equation arises

$$v = \frac{VR_s}{R_s + R_f} \tag{1}$$

It actually relates the measured voltage drop at the ends of a standard resistor (whose electrical resistance is denoted by R_s) with the following quantities: applied voltage (V) and electrical resistance of the investigated thin film sample. In the case of the constant field method, i.e., when $R_s \ll R_f$, eq 1 has the following simpler form

$$v = \frac{VR_s}{R_f} \tag{2}$$

The measurements of temperature dependence of the dark electrical resistance and spectral dependence of photoconductivity were performed using set-ups presented on Figures 1 and 2, respectively, which contain the previously discussed electrical circuit. The temperature dependence of the dark electrical resistance of investigated thin film samples was followed in inert (argon) atmosphere at 80 kPa. In the case of spectral dependence of nonequilibrium conductivity (photoconductivity), a spectrophotometer Beckman DU-2 was used as a source of electromagnetic radiation in the spectral range from 400 to 1200 nm. The ohmic contact with the investigated samples, which is of crucial importance in the process of electrical study, was achieved using coplanar silver electrodes.

The film thickness was determined gravimetrically or interferometrically. It was found that the films deposited from a single reactor were of uniform thickness and density. The thickness of films that were investigated in the present study spanned the range from 50 to 200 nm.

Coherent light-scattering experiments were used to investigate the mechanism of crystal growth during thin film deposition.[26]

4. Results and Discussion

4.1. Chemical Aspects Concerning the Deposition of Low-Dimensional $AgBiS_2$ in Thin Film Form. In this study, the developed experimental routes for synthesis of low-dimensional bismuth(III) silver sulfide thin films follow the general idea of chemical deposition method. The thin-film deposition process is based on controlled precipitation reaction in an acidic aqueous reaction system which begins with dominant homogeneous nucleation, followed by formation of colloidal particles with a relatively narrow size distribution. By means of diffusion, the obtained nanoparticles migrate to the substrate's surfaces where they absorb and coagulate creating thin film of close-packed quantum dots (i.e., a 3D array of $AgBiS_2$ QDs).

In the case of synthesis of semiconducting materials as thin films, the experimental conditions of the deposition process play an exceptionally important role. To obtain thin films with a satisfying quality and higher deposition yield, the rate of precipitation reaction needs to be carefully controlled (i.e., kept at low level). This can be done by controlling the temperature of deposition, the pH of the reaction system or also by maintenance of relevant ion concentrations in the reaction system at low level. In the case of semiconductor under investigation, low concentrations of Bi^{3+} and Ag^+ ions in the reaction system were kept using sodium thiosulfate, which forms complexes with these ions with a suitable stability. On the other hand, part of the thiosulfate ions hydrolyze and generate sulfide ions, which are present in low concentration in the reaction system but sufficient to fulfill the thermodynamic conditions for precipitation.

The hydrolysis of thiosulfate ions is accompanied by the following equilibria in the reaction system[33]

$$S_2O_3(aq) + H_2O(l) \rightleftarrows H_2S(aq) + SO_4^{2-}(aq) \tag{3}$$

$$H_2S(aq) + H_2O(l) \rightleftarrows H_3O^+(aq) + HS^-(aq) \quad pK_1 = 6.88 \tag{4}$$

$$HS^-(aq) + H_2O(l) \rightleftarrows H_3O^+(aq) + S^{2-}(aq) \quad pK_2 = 14.15 \tag{5}$$

So, the concentrations of relevant ions (Bi^{3+}, Ag^+, and S^{2-}) in the reaction system are complex functions of the existing

equilibria. The initial concentrations of the used reagents ($AgNO_3$, $Bi(NO_3)_3$, and $Na_2S_2O_3$) and the temperature during the deposition process were optimized in order to obtain as high as possible yield of the studied material in thin film form with maximum photoresponse and, at the same time, in its low-dimensional structure. By controlling the concentrations of relevant ions, we have actually maintained a careful control of the supersaturation ratio value (S) throughout the deposition process:

$$AgBiS_2(s) \rightleftarrows AgBiS_2(aq) \rightleftarrows Ag^+(aq) + Bi^{3+}(aq) + 2S^{2-}(aq) \quad (6)$$

$$S = \frac{c(Ag^+)c(Bi^3)c(S^{2-})^2}{c(Ag^+)_e c(Bi^3)_e c(S^{2-})_e} = \frac{c(Ag^+)c(Bi^3)c(S^{2-})^2}{K_s} \quad (7)$$

where c_e corresponds to ionic concentrations in the case of saturated solution. Achievement of this goal is very important since this quantity is closely related to the crystal size. Too large values of S would lead to predominant deposition of bulk precipitate, whereas too small values of this quantity would lead to larger crystal size of the deposited material. We have achieved further reduction of the crystal size of synthesized semiconductor by a continuous irradiation of the reaction systems by ultrasound (i.e., employing sonochemical synthetic routes). This is described in more detail in the following chapter.

Regarding the mechanism of crystal growth, on the basis of performed light scattering experiments, we concluded that the crystal growth occurs mainly according to the cluster (or colloidal) mechanism.[34] It can be presented by the following equation:

$$(AgBiS_2)_l + (AgBiS_2)_k = (AgBiS_2)_{l+k} \quad l,k > n \quad (8)$$

where n is the number of formula units which form a stable nucleus. This conclusion is in agreement with other results obtained on the basis of structural investigations of studied material.

In this context, one additional aspect, which is of substantial importance for the nanocrystalline nature of the synthesized material and the evolution of the crystal size upon postdeposition annealing treatment, seems to be worth mentioning. In acidic medium, thiosulfate anions undergo slow hydrolysis, generating colloidal elemental sulfur

$$S_2O_3(aq) + 2H^+(aq) \rightarrow H_2S_2O_3(aq) \rightarrow S(s) + SO_2(g) + H_2O \quad (9)$$

It is likely that such generated colloidal sulfur acts as a capping agent, leading to deposition of ultrasmall $AgBiS_2$ QDs in thin film form and as bulk precipitates as well. The subsequent significant increase in the average QD size upon thermal treatment at relatively modest temperatures could also be related to the association properties of the elemental sulfur.

4.2. Sonochemical Synthesis of Low-Dimensional $AgBiS_2$ in Thin Film Form. As it was previously pointed out, in order to achieve further decrease of crystal size in the studied thin film system compared with the one obtained by a conventional chemical route, we sonificated the reaction system by immersing an ultrasonic horn directly in the minireactor. As it was discussed in the previous paragraph, the crystal growth of $AgBiS_2$ occurred mostly via a cluster (i.e., colloidal) mechanism. Therefore, the reaction system contained phase boundaries (solid–liquid) and the applied ultrasound radiation caused additional effects (so-called heterogeneous sonochemical effects). These, on the other hand, substantially influenced the crystal size of the synthesized nanomaterial.[35,36] In the lack of phase boundaries, the implosive collapse of bubbles, caused under ultrasound irradiation, is a spherically symmetric process. In the opposite case, like the example of our reaction system, the implosion of bubbles in the neighborhood of liquid–solid interfaces is nonspherical and leads to formation of shockwaves and microjets. The shockwaves and microjets could produce many effects because the potential energy of imploded bubbles is converted into kinetic energy. For example, when the exposed solid surface is several times larger than the bubble size, the generated shockwaves and microjets lead to concentration of enormous energy densities at the site of impact. This is accompanied with surface damage, i.e., erosion responsible for ultrasonic cleaning. Otherwise (when the exposed solid surface is smaller than the bubble size), the shockwaves and microjets lead to high-velocity interparticle collisions. These, on the other hand, could result in decreasing or increasing the particle size. The second effect occurs when the energy liberated during the high-energy collisions is large enough to cause local melting of the material nanoparticles. According to the results obtained by Suslik[35,36] and having in mind the cluster mechanism of crystal growth of the investigated semiconductor as well, the surface erosion of nanoparticles, present in the reaction system, does not occur since the frequency of applied ultrasound radiation is 20 kHz. However, the heterogeneous sonochemical effects leaded to a further decrease of nanoparticles' size which was proved by XRD and AFM analyses of the synthesized thin films.

4.3. X-ray Diffraction Analysis of Low-Dimensional $AgBiS_2$ in Thin Film Form. *4.3.1. Identification of Low-Dimensional $AgBiS_2$.* Bismuth(III) silver sulfide is a ternary semiconductor that belongs to the I−V−VI group. It exists in two polymorphic modifications with temperature-dependent thermodynamic stability. At room temperature, the most stable modification is the hexagonal one, whereas at temperatures higher than 200 °C, it crystallizes in the cubic crystal system. The high-temperature modification, which can exist as metastable at room temperature, has rock salt type structure with a unit-cell parameter of 5.648 Å.[37]

On the basis of recorded XRD patterns, it was concluded that the materials synthesized using chemical and sonochemical approaches correspond to the cubic modification of $AgBiS_2$.[38] The recorded diffractograms of as-deposited

(33) *Handbook of Chemistry and Physics*, 64th ed.; CRC Press: Boca Raton, FL, 1983–1984.
(34) Gorer, S.; Hodes, G. *J. Phys. Chem.* **1994**, *98*, 5338.
(35) Suslick, K. S.; Price, G. J. *Annu. Rev. Mater. Sci.* **1999**, *29*, 295.
(36) Suslick, K. S. In *Encyclopedia of Physical Science and Technology*, 3rd ed.; Academic Press: San Diego, CA, 2001.
(37) Gelllr, S.; Wernick, J. H. *Acta Crystallogr.* **1959**, *12*, 46.
(38) JCPDS 89-3672; International Centre for Diffraction Data: Newtown Square, PA.

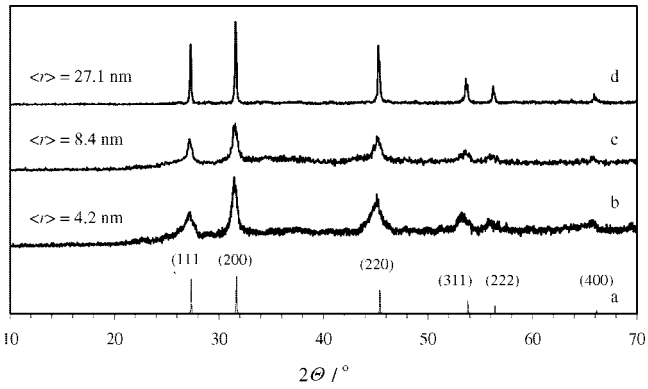

Figure 3. XRD patterns of 3D arrays composed of $AgBiS_2$ nanocrystals: (a) standard, (b) sonochemically prepared, (c) chemically prepared, and (d) thermally treated.

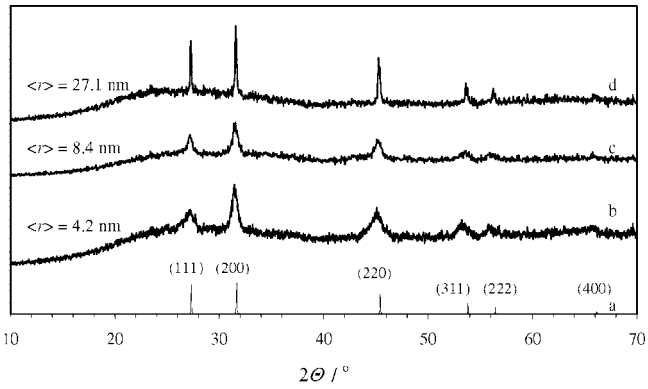

Figure 4. XRD patterns of 3D arrays composed of close packed $AgBiS_2$ QDs deposited as thin films: (a) standard, (b) sonochemically prepared, (c) chemically prepared, and (d) thermally treated.

(chemically and sonochemically) and annealed samples of the obtained semiconductor (as a precipitate and as thin film) are presented on Figures 3 and 4.

As can be seen from the presented XRD patterns, the chemical composition of the synthesized semiconductor does not change upon annealing treatment in air atmosphere at 250 °C.

4.3.2. Crystal Size Estimation. In addition to identification of chemical composition of the synthesized ternary semiconducting material, the recorded XRD patterns were also used for estimation of the average crystal radius in spherical approximation in the framework of Debye–Scherrer method.[39] This model states that the decrease of crystal size in the studied system is accompanied with broadening (so-called intrinsic broadening) of the diffraction peaks in its XRD pattern. The origin of diffraction peak broadening is due to the "relaxed" validity of Bragg's law of diffraction and to the instrumental reasons as well. The relationship between average crystal diameter D (in spherical approximation) and broadening of XRD peaks, according to the previously mentioned model, is quantitatively expressed by the following equation

$$D = \frac{4}{3}\frac{0.9\lambda}{\beta\cos\theta} \tag{10}$$

where λ is the wavelength of the used X-ray radiation, β is the full width at half-maximum intensity of the peak and θ is the angle that corresponds to diffraction maximum. The influence of intrinsic and instrumental broadening of diffraction peaks on crystal size in the Debye–Scherrer equation is included in the following way

$$\beta = \sqrt{\beta_m^2 - \beta_s^2} \tag{11}$$

In the last equation, β_m is the measured half-width of the peak, whereas β_s is the corresponding half-width in the case of an internal (macrocrystalline and strain-free) standard appearing at as close as possible values of θ to that of the peak with a half-width β_m.

The experimental XRD data were processed using the software package GRAMS.[40] The positions and the full widths at half-maximum intensities of the peaks were found by interpolation of diffraction maxima with linear combination of Gaussian and Lorentzian (i.e., Cauchy) functions. The average radius of quantum dots was estimated by averaging the values obtained on the basis of all XRD peaks and on the basis of the slope of $\cos\theta = f(1/\beta)$ dependence as well, using linear interpolation of experimental data

$$D = \frac{4}{3}0.9\lambda\left(\frac{\mathrm{d}\cos\theta}{\mathrm{d}(1/\beta)}\right)^{-1} \tag{12}$$

The estimated average crystal radius of the as-deposited $AgBiS_2$ thin films by chemical route is 8.4 nm. Upon thermal treatments of investigated samples at 250 °C for 1 h the average crystal radius increases to 27.1 nm. This is closely related with the phenomena of coalescence and crystal growth which had been occurring during the annealing treatment. According to the obtained results for crystal size of sonochemically prepared samples, the sonification of the reaction system was proved to be useful synthetic tool for preparation of lower-dimensional structure of investigated material than the one obtained without ultrasound irradiation. The estimated average crystal radius of sonochemically prepared sample of $AgBiS_2$ was two times smaller, i.e., 4.2 nm.

On the other hand, regardless on the employed synthetic method (with or without sonification of the reaction system), the estimated average crystal radius of the obtained semiconductor in thin film form and as a precipitate from the same reaction system was found to be the same. This is in agreement with the results obtained on the basis of light-scattering experiments concerning the cluster mechanism of crystal growth.[29,34]

4.4. AFM Studies of Thin Films' Surface Morphology. Atomic force microscopy (AFM) studies of the surface morphology of as-deposited films prepared by sonochemical and chemical routes were carried out in order to prove the conclusions drawn on the basis of the X-ray diffraction data. Figures 5a and 6a show three-dimensional images of a sonochemically and a chemically deposited $AgBiS_2$ thin film, respectively. Large scale fluctuations are seen whose lateral size is ~50 nm but their vertical amplitude is below 10 nm. The root-mean-square (rms) roughness determined for samples with similar thickness does not significantly depend on the preparation route. A fine

(39) Weller, M. *Inorganic Materials Chemistry*; Oxford Science Publications: Oxford, U.K., 1994.

(40) *GRAMS/32 Spectral Notebase*, version 4.10; Galactic Industries: Salem, NH, 1996.

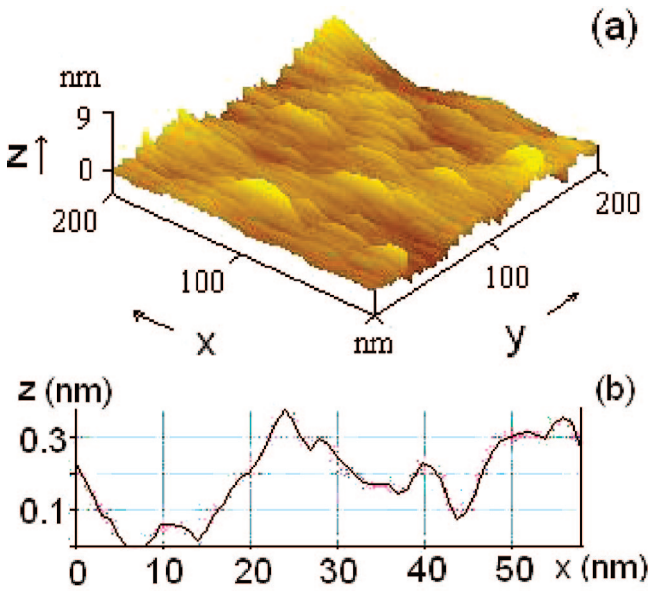

Figure 5. (a) Three-dimensional AFM image of the surface of a $AgBiS_2$ as-deposited thin film prepared with the sonochemical route; (b) surface relief along an occasional line parallel to the *x*-axis.

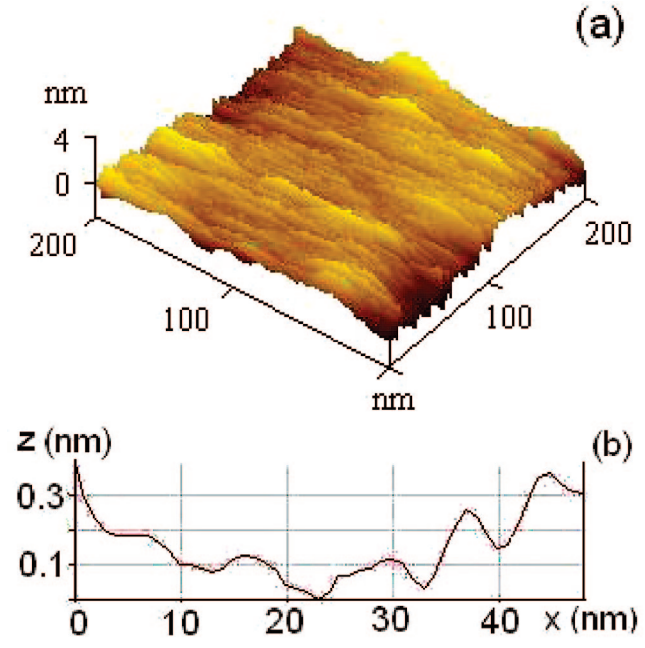

Figure 6. (a) Three-dimensional AFM image of the surface of a $AgBiS_2$ as-deposited thin film prepared with the chemical route; (b) surface relief along an occasional line parallel to the *x*-axis. The axes coincide with those shown in Figure 5.

structure is also seen superimposed on the large scale fluctuations. It indicates the existence of very small grains and proves the nanocrystalline structure of the films assumed on the basis of the X-ray diffraction data. Although the exact value of the grain size cannot be precisely determined, a rough estimation of the size gives values between 5 and 10 nm (see also Figures 5b and 6b). Comparing the surface relief shown in Figure 5b and 6b, one can think that (qualitatively) the grain size in the sonochemically deposited films is smaller than that in the chemically deposited ones. Both observations confirm the conclusions drawn from the X-ray diffraction data.

4.5. Optical Properties of Thin Films Composed of 3D Assemblies of Close-Packed $AgBiS_2$ QDs. Optical properties of the prepared thin films were investigated by absorption spectroscopy. The measured spectral dependencies of transmission coefficient were used for construction of the spectral dependence of absorption coefficient having in mind the following relation between the two mentioned coefficients

$$\alpha(h\nu) = \frac{1}{d}\ln\frac{I_0(h\nu)}{I(h\nu)} = \frac{1}{d}\ln T^{-1}(h\nu) \qquad (13)$$

In the last equation, $h\nu$ is energy of incident photons, wherease d denotes the film's thickness. The last quantity was measured either gravimetrically or interferometrically.

The experimental absorption spectra, i.e., spectral dependences of absorption coefficient, were interpreted in the framework of band theory of solid state,[1–8] also accounting for the nanocrystalline, i.e., low-dimensional, character of the studied systems. The electronic energy structure (band structure) of a solid-state substance is closely related with its crystal structure. Actually, the band structure is a function of a three-dimensional wave vector ($\vec{k}$) within the Brillouin zone, which, on the other hand, depends on the crystal structure and corresponds to a Wigner−Zeits-type primitive unit cell of the reciprocal lattice. According to the mentioned theory, the spectral dependence of absorption coefficient is a complicated function, which involves many parameters related with the nature of investigated system.[41] However, if the investigated system belongs to the group of semiconductors with supposed spherical symmetry of its bands, this relation could be rewritten in simpler way in terms of the semiconductor absorption function, which is more useful in the course of interpretation of the obtained results

$$(\alpha(h\nu)h\nu)^n = \text{const.}(h\nu - E_g) \qquad (14)$$

In the last equation, E_g denotes the band gap energy of the investigated semiconducting system, while the exponent n depends on the type of electronic transitions. When a direct-type of semiconductor (whose valence band absolute maximum and conduction band absolute minimum correspond to same point of *k*-space) is in question, the interband transitions are not accompanied with change of electronic momentum. Consequently, the exponent n could take two values, either 2 or 2/3. In the first case, electronic transitions are dipole-allowed, whereas in the second one, they are dipole-forbidden. Otherwise, when the considered semiconductor has indirect band structure, i.e., when valence band maximum and conduction band minimum correspond to different points in *k*-space, the interband transitions are accompanied by a change in electronic momentum. According to the laws of conservation of energy and momentum, indirect band to band electronic transitions are phonon assisted. This means that such transitions take place involving lattice phonons, which in fact supply the necessary momentum and have a negligible energy compared with E_g. The exponent n takes the value of 1/2 or 1/3 for dipole-allowed and dipole-forbidden indirect electronic transitions respectively. Also, it is worth pointing out that the considered

(41) Pejova, B. In *Progress in Solid State Chemistry Research*; Buckley, R. W., Ed.; NOVA Publishers: New York, 2007.

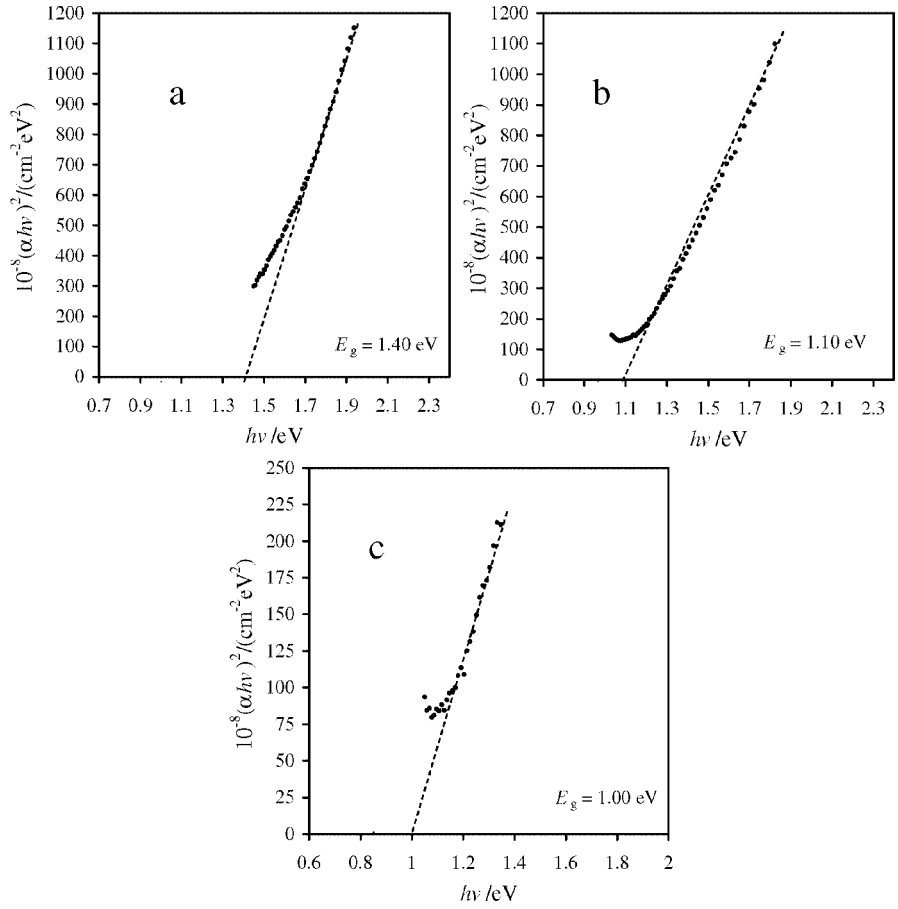

Figure 7. Constructed $(\alpha(h\nu)h\nu)^2 = f(h\nu)$ dependence for (a) nanostructured $AgBiS_2$ thin film prepared by sonochemical deposition; (b) nanostructured $AgBiS_2$ thin film prepared by chemical deposition; and (c) $AgBiS_2$ thin film sample thermally treated in air atmosphere at 200 °C for 1 h, together with the extrapolations to $\alpha(h\nu)h\nu = 0$ and the calculated band gap energies.

equation does not take into account electrostatic interaction between photogenerated charge carriers.

Having in mind the previously outlined arguments, using experimental data for spectral dependence of absorption coefficient for prepared thin films, we constructed semiconductor absorption functions for all physically acceptable values of the exponent n. By a careful analysis of these functions, we concluded that the investigated system belongs to the group of semiconductors with direct band structure. The corresponding direct dipole-allowed band to band electronic transitions start to occur upon interaction with photons from visible part of the electromagnetic radiation spectrum. The band gap energy of the synthesized 3D arrays of close packed $AgBiS_2$ QDs in thin film form was determined by careful analysis of $(\alpha(h\nu)h\nu)^2 = f(h\nu)$ dependence on the basis of a combined interpolation-extrapolation procedure. Since the dispersion relation does not follow parabolic approximation (on which the previously considered form of the semiconductor absorption function is based) in the neighborhood of first Brillouin zone borders, we carried out a linear least-squares fit of $(\alpha(h\nu)h\nu)^2 = f(h\nu)$ dependence by successive inclusion or elimination of a number of neighboring points in wide relevant energy range and at the same time kept an eye on the value of R^2. After that, the linear dependence was extrapolated to $(\alpha(h\nu)h\nu) = 0$ and band gap energy was calculated on the basis of obtained equation. The constructed $(\alpha(h\nu)h\nu)^2 = f(h\nu)$ dependences for both types of thin film samples (prepared sonochemically and chemically) and the corresponding extrapolations are presented on panels a and b in Figure 7. Eventually, following the previously mentioned procedure, we calculated the band gap energies of both sonochemically and chemically prepared samples of $AgBiS_2$ thin films. The values of investigated quantity are 1.40 and 1.10 eV, respectively. These results are in line with those obtained on the basis of XRD analysis (for crystal size estimation) and with our efforts to prepare nanocrystalline samples with as low as possible average crystal size. The calculated values of band gap energy are higher than the one that corresponds to macrocrystalline sample of investigated semiconductor (0.9 eV). This difference is much more pronounced in the case of samples obtained under sonification of reaction system which is due to the previously discussed mechanism of ultrasound influence on crystal growth. On the other hand, because of size quantization effects in the case of low-dimensional systems (with crystal size comparable to Bohr excitonic radius), the crystal size reduction is actually expected to be accompanied with band gap broadening. As an additional means of controlling the crystal size of the synthesized samples (besides by managing the experimental conditions of the deposition process), we have also used a postdeposition annealing treatment. According to the previously outlined results from the structural studies, the crystal size gradually increases under postdeposition annealing

influence. We demonstrate in this chapter that these structural changes are followed by band gap narrowing, which eventually converges toward the bulk value. The $(\alpha(h\nu)h\nu)^2 = f(h\nu)$ dependence in the case of thermally treated sample in air atmosphere at 200 °C for 1 h (presented on Figure 7c) clearly proves the previous statement. Therefore, both of the proposed deposition techniques (chemical and sonochemical), combined with postdeposition treatment, provide a possibility to control the crystal size of the investigated 3D arrays of $AgBiS_2$ QDs deposited as thin films, i.e., to design this material according to an application point of view.

As was mentioned in the introduction, it is a particularly important task to provide novel ways of building of close packed solids from semiconductor QDs. Tailoring the dot size and spacing between QDs in such solids, on the other hand, provides new opportunities to engineer the electronic, optical, and structural properties of semiconductors on the nanometer scale. As we have demonstrated up to this point in this chapter, the proposed synthetic approaches, combined with appropriate postdeposition treatments, enable tunability of linear optical properties of the studied QD thin films. In the following, we will focus on some aspects related to collective properties of the synthesized QD solids and the collective physical phenomena developing upon mutual interaction of the proximal QDs. The first issue that we focus on, in this context, is the absence of clearly defined excitonic absorption peaks (bands) in the measured spectral dependencies of the absorption coefficient of the synthesized QD thin films. In fact, such features are expected to be observed in the case of individual QDs, as the electronic energy structure is discretized because of 3D confinement of charge carrier motions within a QD. This property of individual QDs has been demonstrated many times in cases of colloidal QDs in solutions or in cases of diluted QD ensembles (where the dilution is achieved by appropriate capping ligand).[9–16] However, when isolated QDs are brought in contact, interdot electronic coupling effects occur. Such coupling leads to formation of collective electronic states in an ensemble of quantum dots. The meaning of collective in this context is that these states are delocalized within a finite number of nanocrystals of the 3D QD array. The exact mechanism of interdot coupling is still a subject of many debates, since it depends on the interdot distances and the particular material from which the dots are formed. However, it seems that in cases when QDs are very closely packed (i.e., there is not actually organic or capping layer between the dots), the tunneling mechanism is effectively responsible for charge carrier coupling phenomena. We therefore conclude that the observance of structureless absorption spectra in the studied 3D arrays of $AgBiS_2$ QDs deposited as thin films may be attributed to the formation of collective electronic states in ensembles of quantum dots. Besides this reason, however, the size distribution of the synthesized $AgBiS_2$ QDs could also affect the smearing of the electronic absorption spectra of the films in the region just around the band gap energy. The chemical and sonochemical deposition techniques employed for QD synthesis in the present study, based on colloidal precipitation in acidic medium do not generate highly monodispersed QDs. Accounting for the fact that the QD sizes span the range which is close to Bohr excitonic radius for this material, the 3D size quantization effects could be clearly manifested in the optical absorption of the dots. The observed optical absorption spectrum of the 3D assembly of QDs, deposited as thin films, is therefore actually a convolution of the probability distribution function characterizing the size distribution and the semiconductor optical absorption function including the contribution of the excitonic density of states (in which the size-dependence of the band gap energy is explicitly accounted for). Depending on the exact form of the size distribution function (especially the dispersion in the distribution), it could certainly also add to the smearing of the individual excitonic absorption peaks in the optical absorption spectra.

The second issue that we are going to pay attention to in this context governs the dependence of oscillator strength of the observed electronic transitions on the QD size. Comparison of the plots of $(\alpha h\nu)^2$ vs $h\nu$ in the cases of as-deposited (chemically and sonochemically) and thermally annealed films composed by 3D arrays of $AgBiS_2$ QDs (Figure 7a−c), indicates that the magnitude of absorption coefficient α at a given photon energy decreases upon average crystal size increase. Similarly to the size-induced band gap variation, this is also a quantum effect. Although the size dependence of the exciton oscillator strengths in the case of nanocrystalline semiconductors is still only a partially solved problem, the following arguments may be outlined to explain the experimentally observed trend in our case. As shown by Wang and Herron,[42] the oscillator strength f of the exciton is given by the expression

$$f = \frac{2m}{\hbar^2}\Delta E|\mu|^2|U(0)|^2 \qquad (15)$$

In the last equation, m is the electron mass, ΔE the energy of the transition, μ is the transition dipole moment; $|U(0)|^2$ represents the probability of finding the electron and hole at the same site (a factor of overlap). In the case of a finite size cluster, the absorption coefficient is proportional to the ratio of the overall (total) oscillator strength per cluster - $f_{cluster}$ and the cluster volume V (i.e., $f_{cluster}/V$). As shown elsewhere,[43] two cases may be distinguished with respect to the natural length scale governing the size quantization phenomena. In the case when clusters' radius is larger than the Bohr exciton radius (i.e., $R \gg r_B$), the overlap factor $|U(0)|^2$ is size-independent. In such case, the macroscopic transition dipole moment completely determines the oscillator strength. In the second case (when $R < r_B$) the value of $|U(0)|^2$ increases upon cluster volume decrease and it thus follows that $f_{cluster}$ value is very weakly dependent on the cluster size in this regime. According to this, it could be concluded that the absorption coefficient itself (i.e., the ratio $f_{cluster}/V$) is expected to increase upon cluster size decrease. Such a trend is exactly observed in our experiments, despite the fact that the absorption bands corresponding to excitonic transitions are wiped away by the continuum absorption, as discussed before. It is important to point out in this context

(42) Wang, Y.; Herron, N. J. *Phys. Chem.* **1991**, *95*, 525.
(43) Ueda, Y.; Furuta, A.; Okuda, H.; Nakatake, M.; Sato, H.; Namatame, H.; Taniguchi, M. *J. Electron. Spectrosc. Relat. Phenom.* **1999**, *101–103*, 677.

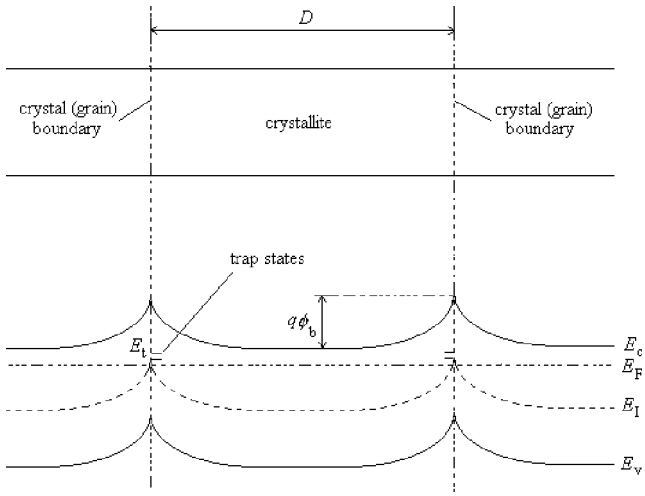

Figure 8. Simplified pictorial presentation of surface band bending, leading to formation of an energetic barrier to intercrystalline charge transport in the case of an n-type semiconductor.

that the described effect of absorption coefficient decrease upon average crystal size increase in the present case is not due to variations in film thicknesses or packing densities of the QDs forming the films. This is so since, as discussed previously, none of these parameters depends on the post-deposition annealing treatment of the films (it is only the QD size that changes upon annealing). Our findings are in line with those described in ref. 42, which further confirms the described trend to be a more general property of QD assemblies.

4.6. Electrical and Photoelectrical Properties of Thin Films of $AgBiS_2$ Quantum Dots. The as-deposited thin films, synthesized by both sonochemical and chemical approaches, are characterized with high electrical resistance (at room temperature). This finding is in agreement with the profoundly manifested nanocrystalline and low-dimensional character of their crystal and electronic structure. In the present study, we have considered several aspects related to charge carrier transport phenomena through 3D arrays of close packed $AgBiS_2$ QDs deposited in thin film form. The first aspect concerns the transport properties of equilibrium charge carriers. The second one, on the other hand, is related to nonequilibrium (i.e., photogenerated) charge carriers (under the conditions when internal photoelectric effect is manifested in the studied nanostructures). As mentioned before, electrical measurements were carried out in the region of ohmic conductivity of the samples i.e. avoiding the effects related to large current injection directly from the electrodes (e.g., the SCLC). This enabled us to focus on the processes of thermal and photoexcitation of charge carriers inherent to the nanostructured films.

Upon annealing treatment of the investigated samples (which is followed only by crystal size enlargement and not by any changes in chemical composition of the films, as shown by structural studies), we detected a pronounced decreasing trend of films' electrical resistance. The as-deposited thin film samples of investigated semiconductor are characterized by dark electrical resistance of the order of GΩ/□ (at room temperature). Upon thermal treatment, this quantity decreases for 2 orders of magnitude (again, measured at room temperature after a heating−cooling cycle). It is reasonable to assume, according to the mentioned observations, that the charge transport processes through the synthesized 3D assemblies of $AgBiS_2$ QDs in thin film form are limited by grain boundary effects, i.e., these processes are barrier-dominated. The more exact proof of the previous statement will be provided further in the context of this section. We will also get a further insight into the main mechanism that governs the intercrystalline charge transfer dynamics through the synthesized 3D nanocrystalline assemblies at room temperature. Assuming therefore a barrier-dominated conductivity of the films of the form[27,44–50]

$$\sigma(T) \propto D\exp\left[-\frac{E_b}{k_B T}\right] \tag{16}$$

where D is the average crystal size and E_b the intercrystalline barrier height, we arrive at the following ratio of thin film conductivities before and after annealing treatment

$$\frac{\sigma_{\text{as-dep.}}}{\sigma_{\text{annealed}}} = \frac{D_{\text{as-dep.}}}{D_{\text{annealed}}}\exp\left[\frac{E_{b,\text{annealed}} - E_{b,\text{as-dep.}}}{k_B T}\right] \tag{17}$$

It can be therefore concluded that the decreasing trend of films' resistivity is due to both crystal size increase and intercrystalline barrier height decrease. A simplified pictorial presentation of surface band bending, leading to formation of an energetic barrier to intercrystalline charge transport in the case of an n-type semiconductor is shown in Figure 8. Since we have determined D values from the analysis of XRD data, using eq (17) we were able to subsequently calculate the decrease in E_b upon thermal treatment of the films. According to eq 17, the ΔE_b value ($\Delta E_b = E_{b,\text{as-dep.}} - E_{b,\text{annealed}}$) is 0.09 eV.

The results from our investigation related to the dominant type of charge carriers (by the hot point probe method) showed that the investigated semiconductor is n-type.

We have further followed the temperature dependence of electrical conductivity of the nanostructured films. A typical temperature dependence of dark electrical resistance (measured in inert argon atmosphere) for one of the investigated samples is presented in Figure 9. The exponential decrease of electrical resistance upon temperature increase is related to the semiconducting nature of investigated system, i.e., with an increase in the concentration of free charge carriers (holes and electrons). The free charge carriers are generated as a result of interband electronic transitions between valence and conduction band or as a consequence of ionization of impurity levels present in forbidden band (the band gap states). The measured data from temperature dependence of dark electrical resistance were interpreted in the framework of solid-state theory for semiconducting materials. In the case of macrocrystalline semiconductors, in which the charge carrier transport may occur through delocalized conduction

(44) Seto, J. Y. W. *J. Appl. Phys.* **1975**, *46*, 5247.
(45) Sharma, R. P.; Shukla, A. K.; Kapoor, A. K.; Srivastava, R.; Mathur, P. C. *J. Appl. Phys.* **1985**, *57*, 2026.
(46) Baccarani, G.; Riccò, B.; Spadini, G. *J. Appl. Phys.* **1978**, *49*, 5565.
(47) Ginger, D. S.; Greenham, N. C. *J. Appl. Phys.* **2000**, *87*, 1361.
(48) Orton, J. W.; Goldsmith, B. J.; Powell, M. J.; Chapman, J. A. *Appl. Phys. Lett.* **1980**, *37*, 557.
(49) Mott, N. F. *J. Non-Cryst. Solids* **1972**, *8–10*, 1.
(50) Orton, J. W.; Powell, M. J. *Rep. Prog. Phys.* **1980**, *43*, 1267.

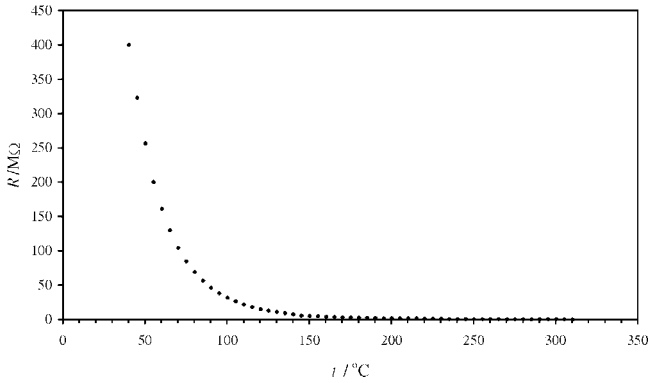

Figure 9. Temperature dependence of dark electrical resistance (measured in inert argon atmosphere) for investigated $AgBiS_2$ thin film sample.

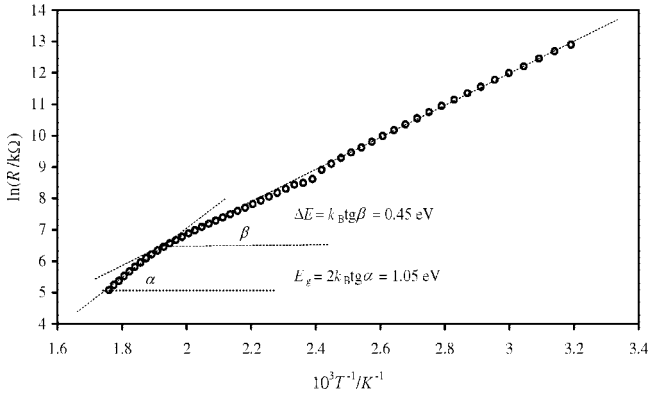

Figure 10. Constructed $\ln R = f(T^{-1})$ dependence for investigated $AgBiS_2$ thin film sample.

band states, either upon their excitation from the valence band or from each of the n distinct discrete band gap states, the temperature dependence of dark (equilibrium) conductivity σ is described with the following function[1–8]

$$\sigma(T) = \sigma_0 e^{-E_g/2k_B T} + \sum_{i=1}^{n} \sigma'_{0,i} e^{-\Delta E_i/k_B T} \qquad (18)$$

where σ_0' and $\sigma_{0,i}'$ are constants, ΔE_i is ionization energy of i-th impurity level from forbidden gap, whereas other symbols have their usual meaning. The function in the eq 18 implies an $(n + 1)$-channel conduction mechanism. Generally, the electrical conductivity depends on two parameters: concentration of free charge carriers and their mobility as well. Although both of the mentioned quantities are temperature-dependent, usually the temperature dependence of mobility is much less pronounced. Therefore, the considered eq 18 has actually been derived assuming a negligible temperature dependence of charge carriers' mobility. In the case of semiconductors with an appreciable degree of disorder, the situation is somewhat more complicated, as discussed further below.

On the basis of performed measurements of temperature dependence of dark electrical resistance, the $\ln R = f(T^{-1})$ dependence for investigated samples was constructed. As could be seen from Figure 10, two linear trends in the explored temperature region (from room temperature to 310 °C) appear. The linear trend from considered dependence in lower-temperature region (∼20−210 °C) is close related with activation of extrinsic conductivity mechanism, whereas in higher-temperature one (∼210−310 °C) it is due to intrinsic type of conduction.

Since the linear trend from the higher temperature region is due to interband electronic transitions, the corresponding experimental data were used for calculation of band gap energy (E_g) of investigated semiconductor. The experimental data were least-squares fitted by the following function

$$\ln R(T) = \frac{E_g}{2k_B}\frac{1}{T} + \ln R_0' \qquad (19)$$

On the basis of the slope obtained by linear interpolation of the experimental data for $\ln(R)$ vs $1/T$ dependence in this temperature region, a value of 1.10 eV for E_g was calculated. The calculated value of band gap energy corresponds to temperature of 0 K[26–29] and it is in agreement with the one obtained for thermally treated samples (prepared by both sonochemical and chemical approaches) using absorption spectroscopy technique.

Concerning the lower temperature region of the measured R vs T dependence, since in the present case we deal with nanocrystalline thin films, one can expect quite a high density of localized states in the forbidden gap, the situation being close to that in amorphous semiconductors. This implies existence of band tails accompanied by a number of other donorlike and acceptorlike defect states in the band gap. These states are usually not expected to be discrete, but to be characterized by some distribution function (e.g., normal, i.e. Gaussian). The dark conductivity of polycrystalline n-semiconductor is proportional to n (i.e., $\sigma = en\mu$, where e is the electron charge, μ the drift mobility, whereas the concentration of the dominant charge carriers is a temperature dependent quantity $n \sim \exp[-E_d/(k_B T)]$). The quantity E_d is the sum of grain boundary barrier height and the Fermi level energy E_F. (i.e., the energy distance between the Fermi level and conduction band bottom), $E_d = E_b + E_F$. Having this discussion in mind, the experimental data from the lower temperature region were interpolated with a function of the form:

$$\ln R(T) = \frac{E_b + E_F}{k_B}\frac{1}{T} + \ln R_{0,1}' \qquad (20)$$

From the slope of the interpolating linear function (in the least-squares sense), a value of 0.45 eV was obtained for the sum of the Fermi energy and the barrier height. Assuming that the grain boundary barrier height in the annealed films is negligible (∼0 eV) the previously mentioned value of 0.09 eV could be related to the barriers in the as-deposited ones. In such a case, a value of ∼0.35 eV could be obtained for the Fermi energy level in the as-deposited films.

In this context, we have also analyzed to some extent certain aspects related to the charge carrier transport mechanism in the synthesized 3D assemblies of $AgBiS_2$ QDs deposited in thin film form. These conclusions could be derived by additional analyses of the measured temperature dependence of electrical conductivity of the films. In case of a QD ensemble (deposited as a macroscopically continual thin layer) the electrical transport is often barrier-dominated. On the basis of observed annealing treatment influence on the electrical conductivity, we have already indicated that it

is certainly the case in our synthesized samples. Inside each nanocrystal, which is a part of the 3D assembly, the atomic arrangements are periodic (resembling those of a macrocrystalline solid), with a more or less pronounced size-induced lattice strain.[32,41] The intercrystalline boundary, on the other hand, represents a complex structure, often containing few layers of disordered atoms, which form a transitional region between the neighboring nanocrystals (with different orientations). The grain boundary influence on the charge carrier transport properties of semiconductors is manifested through the influence of these regions on the bulk electronic band structure of these materials. Within the language of solid-state physics, the potential barriers at the intercrystalline borders arise due to bending of energy bands at the surfaces of nanocrystals (Figure 8). Three possible mechanisms, governing the charge carrier transport through the grain boundaries, have been recognized:[44–51] (i) the variable range hopping (VRH) conduction, (ii) thermionic emission (TIE), and (iii) quantum mechanical tunneling through the barrier (QMT). To determine which of the mentioned mechanisms dominates in the case of presently studied system (in the temperature range in which measurements have been performed), we have applied the approach based on various extensions of the model of Seto[44,46] and other literature models aiming to rationalize the charge carrier transport properties.[45,47–51] The VRH mechanism, following Mott,[49] generates a linear dependence of $\ln[\sigma(T)T^{0.5}]$ on $T^{-0.25}$, i.e.

$$\ln[\sigma(T)\sqrt{T}] \propto T^{-1/4} \tag{21}$$

TIE mechanism, on the other hand, leads to linear dependence of either $\ln[\sigma(T)T^{0.5}]$ or $\ln[\sigma(T)T^{2.5}]$ on T^{-1}, depending on the relative position of trap levels to the Fermi level[44,46]

$$\ln[\sigma(T)\sqrt{T}] \propto T^{-1} \tag{22}$$

$$\ln[\sigma(T)T^{5/2}] \propto T^{-1} \tag{23}$$

The QMT mechanism, finally, would lead to linear relationship between $\sigma(T)$ and T^2

$$\sigma(T) \propto T^2 \tag{24}$$

We have replotted the experimental $\sigma(T)$ data and constructed the functions (21)–(24). The best correlation in the lowest temperature region was found in the case of VRH mechanism (Figure 11). This is not surprising, because according to Orton and Powell,[50] the temperature range over which the VRH mechanism will predominate in the overall conductivity depends on the magnitude of the Debye length (L_D) relative to the crystal size (i.e., crystal diameter D). The Debye length is given by

$$L_D = \left(\frac{\epsilon_r \epsilon_0 k_B T}{e^2 N}\right)^{1/2} \tag{25}$$

where ϵ_r is the static relative dielectric constant of the investigated material, N is the doping concentration, while all other symbols have their usual meanings. In case when $D \ll L_D$, the crystals constituting the 3D assembly of QDs (polycrystalline sample) are almost entirely depleted and we

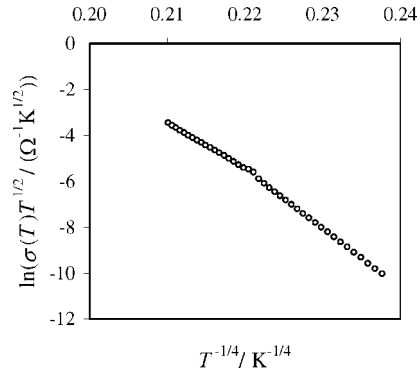

Figure 11. Constructed $\ln[\sigma(T)\sqrt{T}] = f(T^{-1/4})$ dependence for investigated $AgBiS_2$ thin film sample.

expect the VRH conduction mechanism to be effective over a considerably wide temperature range. Contrary to the case of amorphous materials, the VRH conduction mechanism in polycrystalline samples occurs at crystal boundaries at temperatures for which the charge carriers do not acquire sufficient energy to cross the potential barrier by thermionic emission. Instead, they are transferred from a charged trap state to a neutral trap state. Note that the TIE dependencies also allow a fairly well fit of the experimental data (the quality of fit is actually comparable with that for the VRH mechanism), which indicates that this mechanism could certainly also significantly contribute to the intercrystalline charge carrier drift. In fact, although no definitive quantitative conclusions about the outlined issues could be obtained from the existing experimental data, the implications concerning the significance of the VRH mechanism in the region of rather high temperatures, which has been in fact implied in earlier works,[50] is in our opinion a rather important one for the physics of 3D QD assemblies. At temperatures higher than 413 K (the kink in dependence presented on Figure 11), other scattering mechanisms may interplay and even become predominant over the grain boundary one. Other authors have also reported kinks in the $\ln[\sigma(T)T^{1/2}]$ vs T^{-1} dependencies in temperature ranges from 350 to 390 K.[52]

In addition to the phenomena related to equilibrium charge carrier transport outlined before, in this study, we have also followed the manifestation of photoconductivity (i.e., nonequilibrium conductivity), σ, in the case of samples prepared by both chemical and sonochemical approaches. The phenomenon of photoconductivity is closely related with generation of nonequilibrium charge carriers upon interaction with radiation from the visible part of electromagnetic spectrum (so-called internal photoelectric effect).[1–8] Keeping in mind the fact that the band gap energy of investigated semiconductor belongs to the visible part of electromagnetic spectrum, we tried to optimize the experimental conditions of the deposition process with respect to the photoconductive properties of obtained films (i.e., defining the photosensitivity as the most important target function).

According to our experimental results, the as-deposited samples did not exhibit photoconductivity. This finding is in correlation with the previously discussed evidence for profound, nanocrystalline structure of synthesized material.

(51) Garcia-Cuenca, M. V.; Morenza, J. L.; Esteve, J. *J. Appl. Phys.* **1984**, *56*, 1738.

(52) Gupta, P.; Chaudhuri, S.; Pal, A. K. *J. Phys. D: Appl. Phys.* **1993**, *26*, 1709.

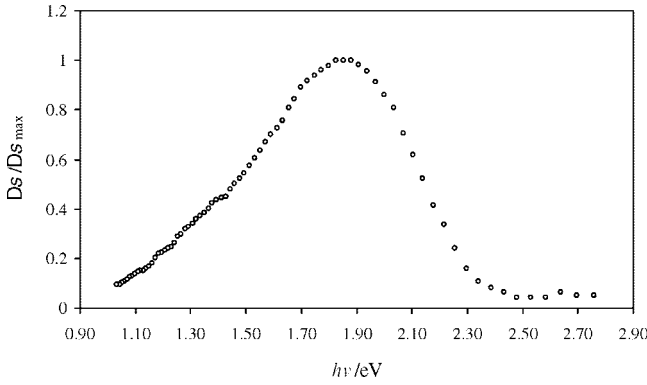

Figure 12. Spectral dependence of stationary nonequilibrium conductivity (photoconductivity) measured by the constant field method for $AgBiS_2$ thin film sample annealed at 250 °C for 40 min.

As it was discussed previously, due to a low-dimensionality of the samples, high intercrystalline energetic barriers to charge carrier transport are formed. From other respect, upon thermal treatments of investigated samples, the average nanocrystal size increases and the grain boundary effects diminish. This results in improvement of electrical contact between nanocrystals and decrease of the density of so-called fast recombination centers and therefore the photoconductive response of the samples (expressed, e.g., through their photosensitivity) is significantly improved. We measured the spectral dependence of the stationary nonequilibrium conductivity (photoconductivity) of annealed samples and used these data to derive more conclusions concerning the mechanism of photoresponse and to calculate the band gap energy from the photoconductivity spectra of these samples. A typical spectral dependence of photoconductivity measured by the constant field method, in the case of a sample annealed at 250 °C for 40 min, is presented in Figure 12. The delta-like shape of the $\Delta\sigma_{st.} = f(h\nu)$ dependence suggests that surface recombination phenomena play a particularly relevant role in the photoconduction process, as shown quantitatively by Devore.[53] The maximal photoresponse of the investigated thin film is manifested at 1.85 nm (the peak in the photoconductivity spectrum), whereas the "red" absorption edge corresponds to about 0.90 eV. On the other hand, photons with energies higher than 1.90 eV cause a considerable reduction of the photoresponse.

According to the previous discussion related to equilibrium charge carrier transport properties, the current flow through the 3D assemblies of $AgBiS_2$ QDs deposited as thin films is modulated by the grain boundary barriers. In other words, the charge carriers have to overcome the boundary barriers that are encountered in the direction of the applied field (drift barriers). The recombination of photogenerated charge carriers is, on the other hand, hindered by recombination barriers which usually lead to spatial separation of the electron–hole pairs. Although certain cases have been reported in the literature demonstrating that these two barriers are different,[52,54–62] some authors have reported that it is one and the same barrier that governs the drift and recombination of charge carriers in some materials.[52,54–62] Using a quantitative formulation of the previous statement, the increase in conductivity upon illumination of the 3D array of QD thin films may be modulated by an increase of the free carriers concentration ($\Delta\sigma_n$) and/or decrease of the grain boundary barrier height ($\Delta\sigma_{E_b}$), i.e.

$$\Delta\sigma = \Delta\sigma_n + \Delta\sigma_{E_b} \tag{26}$$

The second term, arising due to change of grain boundary barrier height upon illumination (ΔE_b), may be considered formally as an increase of the mobility of photogenerated charge carriers in comparison to the case when illumination is absent.[52,54–62] Such consideration enables us to rewrite eq 26 in the form

$$\Delta\sigma = e\mu^*\Delta n + e\mu\Delta\mu^* \tag{27}$$

where n is the charge carrier concentration in the crystallite (grain), and μ^* is their effective mobility. Following the approach given in ref 63, assuming a linear relationship between $-\Delta E_b$ and Φ (i.e., $-\Delta E_b = \Phi$), we rewrite eq 27 including the incident photon flux Φ in the following form

$$\Delta\sigma = e\mu^*\Delta n + \beta\, e\, \mu^*\frac{n}{k_B T}\Phi \tag{28}$$

If the thin film thickness d is much larger than the carrier diffusion length, the excess carrier concentration will be given by

$$\Delta n = \frac{\Phi\tau}{d}[1 - \exp(-\alpha(h\nu)\, d)] \tag{29}$$

where τ is the excess carrier lifetime. However, if this condition is not fulfilled (in our case the carrier diffusion length and film thickness are comparable), the surface and bulk recombination velocities will be comparable. As shown in more detail elsewhere,[63,64] the expression of the form (29) for Δn in such a case will also contain other terms, which will make the function $\Delta n = f(\alpha)$ to go through a maximum and decrease for higher values of α. In other words, the photoconductivity spectral response curve is expected to have a maximum, which is exactly what we observe in our experiments.

Assuming that n and E_b are controlled by a single grain-boundary defect level with an energy E_t below the conduction band, elaborating further the eq 29[63] leads to an expression of the following form describing the spectral dependence of $\Delta\sigma_{st.}$

(53) Devore, H. B. *Phys. Rev.* **1956**, *102*, 86.
(54) Banerjee, N. K.; Chaudhuri, A. K.; Samantaray, B. K. *J. Phys. D: Appl. Phys.* **1993**, *26*, 1714.
(55) Pal, U. *Semicond. Sci. Technol.* **1993**, *8*, 1331.
(56) Datta, S. K.; Chaudhuri, A. K. *Semicond. Sci. Technol.* **1989**, *4*, 376.
(57) Card, H. C. *Solid-State Electron.* **1982**, *25*, 505.
(58) Card, H. C. J. *Appl. Phys.* **1981**, *52*, 3671.
(59) Orton, J. W.; Goldsmith, B. J.; Chapman, J. A.; Powell, M. J. *J. Appl. Phys.* **1982**, *53*, 1602.
(60) Humphrey, J. N.; Petritz, R. L. *Phys. Rev.* **1957**, *105*, 1192.
(61) Petritz, R. L. *Phys. Rev.* **1956**, *104*, 1508.
(62) Slater, J. L. *Phys. Rev.* **1956**, *103*, 1631.
(63) Rakhshani, A. E. J. *Phys.: Condens. Matter* **2000**, *12*, 4391.
(64) Bube, R. H. *Photoelectric Properties of Semiconductors*; Cambridge University: Cambridge, U.K., 1992.

$$\Delta\sigma_{st.} = \frac{e\tau\mu}{d}[1-\exp(-\alpha(h\nu)d)]\exp\left(-\frac{E_b}{k_BT}\right) + \frac{e\beta\mu}{k_BT}\frac{\eta NN_cD}{N_t-DN}\exp\left(-\frac{E_t}{k_BT}\right) \quad (30)$$

In the last equation, N is the doping concentration, N_c is the conduction band density of states, and N_t is the surface density of defect levels at grain boundaries. The quantity η is given by[63]

$$\eta = \frac{k_BT}{E_b}\left[1-\exp\left(-\frac{E_b}{k_BT}\right)\right] \quad (31)$$

Even if we do not account for the more complex dependence of Δn on α (discussed before), the following conclusions based on eq 30 may be derived for the presently studied material. The first term in eq 30 (usually called the ordinary photoconductivity) is proportional to α in the limit of low absorption. The second term, on the other hand, represents the modulated photoconductivity (it arises due to the modulation of E_b by the incident photon flux). As is obvious from Figure 12, small nonequilibrium conductivity is measured at incident photon energies below E_g. This part of the photoconductivity response spectrum could be attributed exactly to the reduced value of the grain boundary barrier E_b upon interaction with light. This modulation of E_b occurs as a result of the sub-band gap transitions involving grain boundary states, which are induced by the incident photon flux.

As discussed in more details in our previous papers,[27,41] in the limit of low absorption of the films ($\alpha d < 1$) there is a direct proportionality between the photoconductivity spectrum (the function $\Delta\sigma_{st.}/\Delta\sigma_{st.,max.} = f(h\nu)$) and the absorption spectrum, i.e., the function $\alpha = f(h\nu)$. Such proportionality arises due to the fact that the $\Delta\sigma_{st.}$ value is proportional to the number of photons absorbed by the investigated thin film, i.e.

$$\Delta\sigma \propto \int_0^d \alpha I_0 \exp(-\alpha x)\,dx = \alpha I_0 \int_0^d \exp(-\alpha x)\,dx \quad (32)$$

Solving the integral in 32 in the limit of low absorption leads to the following relation:

$$\Delta\sigma \propto (1-\exp(-\alpha d)) \approx \alpha d \quad (33)$$

The same conclusion may be derived by analysis of eq 30 in the limit of low absorption. We have used the relation 33 to calculate the band gap energy of the synthesized photoconductive material employing the Fermi's golden rule for band-to-band transitions, within the framework of parabolic approximation for the dispersion relation. In the expressions arising from the Fermi's golden rule, we have simply replaced the function $\alpha(h\nu)$ by $\Delta\sigma_{st.}(h\nu)$ or $\Delta\sigma_{st.}/\Delta\sigma_{st.,max.}(h\nu)$ and constructed the dependencies of $((\Delta\sigma_{st.}/\Delta\sigma_{st.,max.})h\nu)^n$ on $h\nu$ for various values of the exponent n. Clearly manifested linear dependencies of $((\Delta\sigma_{st.}/\Delta\sigma_{st.,max.})h\nu)^n$ on $h\nu$ were observed only for $n = 2$ (Figure 13), which, in line with the optical spectroscopy data, suggests that direct band-to-band electronic transitions contribute to the internal photoelectrical effect. We have carefully carried out linear least-squares interpolations of the $((\Delta\sigma_{st.}/\Delta\sigma_{st.,max.})h\nu)^2$ vs $h\nu$ dependencies in the relevant energy ranges, with successive inclusion or elimination of a number of neighboring points in the correlation ranges and parallel monitoring of the R^2 value. Subsequently, we have extrapolated $((\Delta\sigma_{st.}/\Delta\sigma_{st.,max.})h\nu)^2$ vs $h\nu$ dependencies to $\Delta\sigma h\nu = 0$, which enabled us to determine the corresponding transition energies, on the basis of previously derived correlation equation of the forms

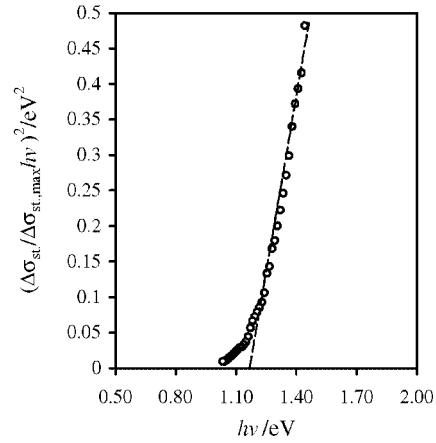

Figure 13. Constructed $((\Delta\sigma_{st.}/\Delta\sigma_{st.,max.})h\nu)^2 = f(h\nu)$ dependence for $AgBiS_2$ thin film sample annealed at 250 °C for 40 min, together with the extrapolation to $(\Delta\sigma_{st.}/\Delta\sigma_{st.,max.})h\nu = 0$.

$$((\Delta\sigma_{st.}/\Delta\sigma_{st.,max.})h\nu)^2 = \text{const.}(h\nu - E_{g,dir.}) \quad (34)$$

The determined value for $E_{g,dir.}$ according to the described procedures was 1.18 eV (Figure 13). It is slightly higher than the one derived from optical absorption spectroscopy data (1.00 eV).

5. Conclusion

As a conclusion, the following points could be summarized:

- A novel, convenient sonochemical approach has been developed that allowed 3D arrays of close packed $AgBiS_2$ quantum dots (QDs) in thin film form to be synthesized for the first time. The proposed sonochemical deposition technique, combined with postdeposition treatment, opens a wide range of possibilities for controllable synthesis of low-dimensional nanostructured films of the investigated semiconductor and to design QD size depending on application point of view.
- The average QD radius of sonochemically synthesized colloidal crystals of this semiconducting material is 4.2 nm, and is two times smaller compared to the value for a QD solid obtained without ultrasonic irradiation of the reaction system.
- The optical band gap energy of sonochemically synthesized as-deposited $AgBiS_2$ QDs (1.40 eV) is strongly blue-shifted in comparison to macrocrystalline value (0.90 eV) and to the value of 1.10 eV for the nanostructured films synthesized by a conventional chemical route from the same reactor. Upon postdeposition annealing treatment, the band gap energy of the films could be red-shifted to 1.00 eV.
- Thermal band gap energy of the films calculated on the basis of temperature dependence of dark conductivity is 1.10 eV, whereas at conditions close to room temperature, the variable range hopping conduction mechanism (along with

the thermionic emission) is predominant in the overall intercrystalline charge carrier transport through the 3D QD assemblies.

• Photoconductivity of the nanostructured $AgBiS_2$ films is modulated by the intercrystalline barrier height decrease upon illumination. The as-deposited films are not photoconductive and they acquire appreciable photoresponse upon annealing treatment, which is accompanied by increase of crystal size and decrease of intercrystalline barrier height by 0.09 eV. The band gap energy of the films calculated on the basis of photoconduction spectral response in the low-absorption region is 1.18 eV.

Acknowledgment. This work has been supported by the Macedonian and Bulgarian Ministries of Education and Science (contract BM-2).

CM071794K